Chapter

The Influence of Interfacial Transition Zone on Strength of Alkali-Activated Concrete

Pavel Krivenko, Oleh Petropavlovskyi, Oleksandr Kovalchuk and Oleksandr Gelevera

Abstract

A process of structure formation taking place in the interfacial transition zone (ITZ) "cement stone-aggregate" was studied on a variety of concretes made with artificial and real aggregates. The study of these processes in the case of artificial aggregate prepared from a mixture of clay loam and alkali-activated slag cement showed that not only active SiO_2 and Na_2O but also other substances of both cement and aggregate are involved in the formation of the ITZ. This results in the formation of alkaline and alkaline-alkali-earth aluminosilicate hydrates which strengthen the ITZ and improve strength and durability of the concrete. Thus, the alkali-silica reaction (ASR) transforms from a destructive one (negative effect) into a constructive one (positive effect). The study on the ITZ in the alkali-activated cement concretes made with real alkali-susceptible aggregates selected from crushed basalt rock, glassy waste product from basalt fiber production, crushed perlite rock, and expanded perlite suggested to make a conclusion on the possibility to prevent the destructive processes in the ITZ through the addition of the metakaolin additive into the cement composition in quantities of 5–10% by mass. These conclusions were supported by the long-term testing of strength of these concretes, by measuring the deformations "shrinkage-expansion" as well as the results of study on hardness of the ITZ.

Keywords: alkali-activated cement, alkali-aggregate reaction (AAR), alkali-silica reaction (ASR), alkali-susceptible aggregate, alkaline and alkaline-alkali-earth aluminosilicate hydrates, basalt rock, interfacial transition zone (ITZ), metakaolin, perlite rock, Portland cement

1. Introduction

Nowadays, concrete is recognized as one of the basic constructional materials. However, strict requirements to its performance properties, in particular durability, are not met in all cases allowing big concerns to occur. With worsening of the ecological situation and larger volumes of use of off-standard materials as concrete constituents, durability became a main criterion of concrete quality. One poorly studied and "hidden" reason explaining low durability of concrete in some cases is the so-called internal corrosion occurring in a cement paste/aggregate interfacial transition zone (ITZ) in concrete, where the cement paste with thicknesses of a few

microns comes into interaction with the aggregate. The ITZ is considered as the strength-limiting phase in concrete.

The ITZ is formed in the process of redistribution of the substances of the cement and aggregate and a result of the reaction "alkali-silicic acid." Depending upon a composition of the formed hydration products, this reaction can be either a destructive (negative effect) one or a constructive (positive effect) one [1–5]. It is believed [6–9] that destructive corrosion of concrete can occur as a result of chemical interaction of alkalis $Na_2O + K_2O$ of the cements with amorphous silica present in particles of aggregates. Not only amorphous silica but also other substances of aggregate constituents—microcrystalline quartz, micas, clay minerals—can enter into interaction with alkalis. This changes a phase composition of the hydration products in the ITZ, resulting in either its weakening or occurrence of critical deformations of expansion. The problem is that these processes are very slow and signs of corrosion can appear after months and in most cases after years of service [9–16].

An alkali can come into concrete in case of cements with the increased contents of alkaline oxides ($Na_2O + K_2O$) (over 0.6%). The higher quantities of alkalis in concrete can be attributed to the wider use of chemical, mineral, and organic additives and admixtures containing them. Alkalis can also come from outside, for example, with seawater, de-icing chemicals, etc. [17, 36–38]. Also, in recent years more and more widely spread are the alkali-activated cements [18–20], in which the alkali contents (1.5–5.5% by mass) are much higher than the values permissible for Portland cements (no more than $NaO + K_2O = 0.6\%$ by mass). This can in the future initiate an alkali-silica reaction (ASR) in case of alkali-susceptible aggregates.

The results of first observations of cases of severe concrete damage as a result of alkali-aggregate reaction were reported by E.A. Stephenson as long ago as in 1916. In 1940 Stanton [21] observed the alkali-aggregate in the concrete used for diverting dam in California. In the recent years, this problem attracted attention of many researchers, which not only studied and continue to study a mechanism of corrosion process but showed main factors which could affect the alkali-silica reaction [1, 39–40]. Among these factors are the higher alkali contents of cement, the higher cement content of concrete, quantity of alkali-susceptible aggregates, temperature and humidity, permeability of concrete, ingress of alkalis from outside, mineral composition of aggregates, etc.

All these allowed to develop measures on how to prevent or weaken the alkali-silica reaction. Among such measures are the use of cements containing additives with latent hydraulic activity or pozzolanic materials, such as granulated blast-furnace slag (GBFS), fly ash, microsilica, volcanic glass, and metakaolin. So, Malek and Roy [22] studied a role of Al_2O_3 and made a conclusion on its positive role in transformation of the ASR from a destructive one into a constructive one. As a result of the so-called "constructive" reaction, the insoluble alkaline and alkaline-alkali-earth aluminosilicate hydrates, analogs to natural zeolites (CaO) $Na_2O{\cdot}Al_2O_3{\cdot}nSiO_2{\cdot}mH_2O$, can be formed in the ITZ. These conclusions were further supported by numerous researchers [23–30], which provided practical solutions on struggle with the ASR through addition in the cement composition of Al_2O_3-containing additives. However, this oxide is contained in aggregates as well [31–35]. For this reason, the structure formation processes in the ITZ flow with participation of not only substances of cement components, but of substances of aggregate constituents as well, which always contain finely dispersed clay particles.

The purpose of this research was to study the influence of the processes flowing in the interfacial transition zone in the alkali-activated cement concretes made with different aggregates on their properties.

2. Materials and testing techniques

In order to study the structure formation processes in the interfacial transition zone, an artificial (model) granular aggregate was used: the granules were prepared from the following mix—clay loam, 75% by mass; granulated blast-furnace slag, 25% by mass; and alkaline component (Na_2CO_3 solution), 15% by mass, without any firing. The preparation process was as follows: all constituents were mixed, and granules 10–20 mm in size were formed, which then were allowed to harden for 28 days in normal conditions.

The concrete cube specimens (10 × 10 × 10 cm) from the alkali-activated cement (granulated blast-furnace slag, 92% by mass, and Na_2CO_3, 8% by mass) and these granules to be used as aggregate were prepared and were subjected to steam curing at t = 90 ± 2°C for 8 h. The ITZ was studied at an age of 28 days.

To study properties of the concrete made using real aggregates, the following cement compositions were chosen:

- Portland cement (OPC) + water
- Alkali-activated Portland cement (OPC + soluble silicate)
- Alkali-activated slag cement (GBFS + soluble silicate)
- Alkali-activated slag cement (GBFS + sodium metasilicate ($Na_2O{\cdot}SiO_2{\cdot}5H_2O$))
- Alkali-activated slag cement (GBFS + sodium carbonate Na_2CO_3)

Used as aggregates were:

- Crushed basalt rock
- Glassy waste product from basalt fiber production
- Crushed perlite rock
- Expanded perlite

Chemical composition of the constituent materials is given in **Tables 1–3**.
The alkaline activators were added in a form of solution; those were:

- Soluble silicate Ms = 2.9. ρ = 1.3 g/cm^3
- Sodium metasilicate ($Na_2O{\cdot}SiO_2{\cdot}5H_2O$) with ρ = 1.25 g/cm^3
- Sodium carbonate (Na_2CO_3) with ρ = 1.18 g/cm^3

Specific surface area of the granulated blast-furnace slag was 300–330 m^2/kg and that of the metakaolin, 1800 m^2/kg.

Grain sizes of the aggregates were within ranges of 3–5 mm.

2.1 Test methods

Thin sections were cut directly from the beam specimens of the composition "cement-aggregate" taken as 1:2 which were used to study the interfacial transition zone.

Material	Mass percentage of oxides								Σ %	M_o	M_a
	SiO_2	Al_2O_3	CaO	MgO	Fe_2O_3	SO_3	$Na_2O + K_2O$	LOI			
GBFS	39.0	5.9	47.7	5.56	0.29	1.48	0.1	0.5	100.53	1.19	0.151
OPC	21.82	5.30	65.91	1.11	4.86	0.99	0.22	0.2	100.41	—	—
Metakaolin	55.05	35.40	3.01	0.92	4.27	0.28	—	0.07	99.00	—	—
Clay loam	92.10	3.50	5.29	—	0.87	—	—	2.12	103.88	—	—

Table 1.
A chemical composition of the constituent materials.

Resulted density, g/cm^3	Silicate modulus	Content calculated on dry matter, g		Mass percentage of oxides			
		In 1 l of solution	In 1 kg of solution	SiO_2	R_2O_3	Na_2O	CaO
1.40	2.96	539.9	385.6	28.5	0.19	9.37	0.15

Table 2.
Characterization of the soluble silicate.

Oxides	Mass percentage of oxides			
	Basalt		Perlite	
	Basalt rock	Glassy waste product from basalt fiber production	Perlite rock	Expanded perlite
SiO_2	50.200	50.050	72.820	76.730
Al_2O_3	14.000	15.350	12.500	13.160
Fe_2O_3	6.340	6.230	0.650	0.680
FeO	8.670	7.000	0.900	0.950
TiO_2	1.620	2.680	0.110	0.110
MnO	0.240	0.300	0.030	0.030
CaO	8.350	9.210	1.070	1.120
MgO	6.600	5.580	0.170	0.180
P_2O_5	0.320	—	0.007	—
K_2O	0.710	0.770	4.510	4.740
Na_2O	2.270	2.180	2.100	2.210
SO_3	0.080	0.150	0.050	0.040
LOI	0.550	—	4.750	—
Σ, %	99.950	99.500	99.667	99.950

Table 3.
Chemical composition of the aggregates.

The ITZ was studied with the help of a scanning electron microscope.

A hardness and elemental distribution in the ITZ were studied as well.

The metakaolin, taken in quantities 5–15% by mass, was chosen as an additive to retard the ASR.

Strength determination was done on beam specimens (4 × 4 × 16 cm) prepared from the concrete mixture "cement-aggregate" taken as 1:2 by mass, except for the specimens made using the expanded perlite as aggregate. Since mean densities of crushed basalt, glassy waste product from basalt fiber production, perlite rock, and cement were more or less close to each other, that of the expanded perlite was different—it was by 10 times lower. For this reason, in order to maintain in all specimens under study an equal volume of cement matrix, the proportions between the cement and expanded perlite in the concrete were taken as 1:0.2 by mass. After preparation, the specimens were kept for 2 days in normal condition and then in a thermostat at temperatures of 20 and 65°C and relative humidity (RH) of about 100%.

Autogenous deformations were measured using a device with a dial indicator with a scale 0.01 mm. The basic measurements were taken at an age of 2 days.

A state of the interfacial transition zones, as was earlier mentioned, is determined, first of all, by the composition and properties of the hydration products as well as by the interface bond strength due to a mutual penetration of the substances of various constituents of the concrete mixture [31, 35]. However, because of small dimensions of the subjects to be studied, the examination of the hydration products in the interfacial transition zones is difficult. For this reason, a spectral imaging in X-ray microanalysis was applied.

The presence and distribution of chemical elements that were supposed to present in the composition of the hydration products, occurring in the interfacial transition zone, was determined using this examination technique [41]. The elemental (Na, Al, Si, and Ca) distribution was done using the X-ray images and their concentrations—by an intensity of the characteristic lines. The concentration curves of elemental distribution were plotted in accordance with the results of qualitative analysis. A width of the section under study was 200 μm. The measurement of microhardness was done with the use of a microhardness measuring apparatus with a diamond pyramid.

3. Results and conclusions

3.1 The structure formation process in the ITZ "alkali-activated cement-alkali-susceptible aggregate"

3.1.1 Concrete mixture "alkali-activated cement-artificial alkali-susceptible aggregate"

The study of the ITZ structure formation in the concrete mixture "artificial granular aggregate-GBFS-Na_2CO_3 solution" taken in the following proportions, 8:1.95:0.5 by mass calculated on Na_2CO_3 dry matter, showed that the highest values of microhardness were characteristic of the interfaces between the cement paste and granules. This can be attributed to strong adhesion of the cementation material to an activated matter of the clay loam-based loamy granules and formation of the hydration products which determine high-performance properties of the concrete. Bond strength in the interfacial transition zones of the steam-cured concrete is 3.8 MPa and after 3 years—4.5 MPa.

The structure of the ITZ in the steam-cured alkali-activated cement concrete at an age of 28 days was dense. The boundary of the interface in some regions discontinues, testifying to a mutual penetration of these regions and blurring the border between the cement stone and aggregate.

The study of the 3-year-old concrete showed that the ITZ in this case is itself a close interlacement of substances included in the cement paste and the granule and

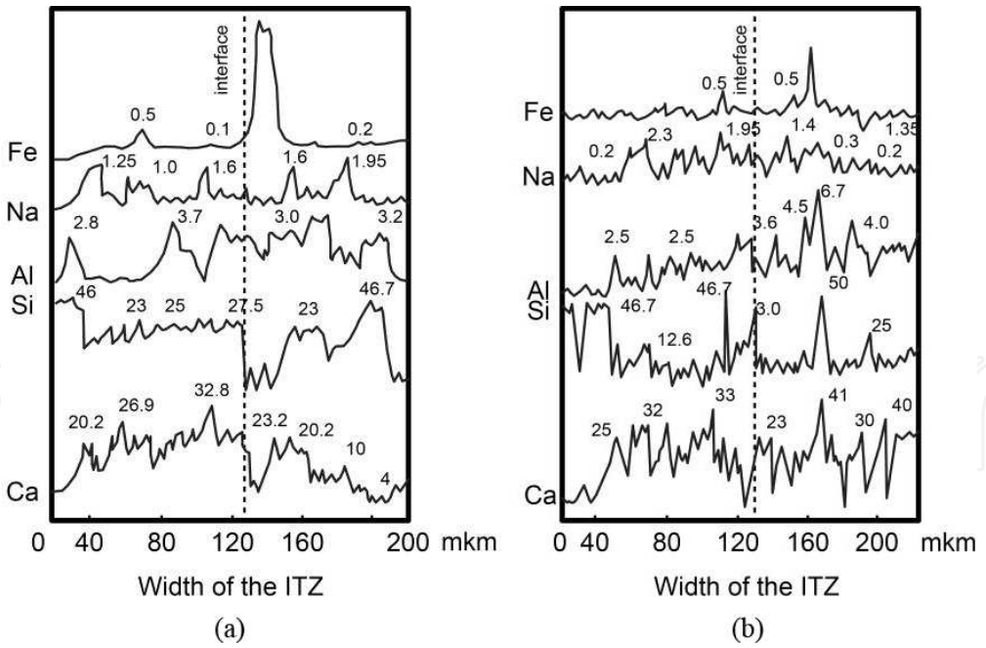

Figure 1.
The concentration curves of elemental distribution in the cement paste/granular aggregate interfacial transition zones in the steam-cured alkali-activated cement concrete: (a) at age of 28 days; (b) at age of 3 years [42].

is characteristic of the presence of the clearly visible (expressed) new phases. The interface is not visible (absent).

A comparative analysis of the obtained concentration curves of elemental distribution (**Figure 1**) suggested to conclude that sodium, aluminum, silicon, calcium, and iron are present over the whole width of the ITZ in the steam-cured alkali-activated cement concrete. Sodium and silicon were distributed homogeneously over the interface, iron is contained in small quantities (**Figure 1a**). The distribution of Ca and Al is inhomogeneous. So, the content of calcium is reducing in two times as far as closer to the granule, and that of aluminum—increasing in the same direct. Evidently, it is attributed to the fact that the hydration products in the cement paste are represented chiefly by low-basic calcium silicate hydrates and partially by the hydrogarnets, so far as the alkaline aluminosilicate hydrates are formed in the granules along with the abovementioned.

On the contrary to the investigated concentration curves of elemental (Ca and Al) distribution in the ITZ of the 3-year-old alkali-activated cement, concrete is characteristic of homogeneous uniform elemental (Ca and Al) distribution over the width of the interface (**Figure 1b**). The earlier observed aggregations of calcium near the cement paste and aluminum granules are absent. Calcium is homogeneously distributed over the interface, and quantity of aluminum approaching to the cement paste of the concrete greatly increased. After 3 years of hardening of the alkali-activated cement concrete, the curves of elemental distribution of all elements are characterized by high-frequency oscillations of concentrations, which can be an evidence of the increase of the interface bond strength and compaction the structure of the interface.

Evidently, change of the state of the ITZ in time can be attributed to physical-chemical processes occurring in the concrete. Above such phenomena as adsorption, diffusion, and others, a chemical interaction of the substances contained in various cements and aggregates took place, leading to formation of the hydration products of the alkaline, alkali-earth, and mixed alkaline-alkali-earth aluminosilicate composition—such compounds like aluminosilicates of sodium and calcium.

The presence of such interaction is supported by the statistical correlation analysis of the obtained data [42]. Analysis of the concentration curves suggested to draw a conclusion on a correlation dependence between the chemical elements in the interface.

The coefficients of correlation were calculated by methods of pair and multiple correlation.

A comparative evaluation of the obtained data showed that in early ages of hardening of the steam-cured alkali-activated slag cement concrete with artificial granular aggregate in transition zone, the elements Na and Si, Al and Si, Al and Ca, Na and Al, and Ca and Si are combined; their coefficients of pair correlation are significant. The closest bound in that case characterizes a coefficient of pair correlation for Si and Ca, which amounts for 0.782 before interface line and 0.689 after the interface line. This can serve as evidence of the presence of calcium silicates in the ITZ. However, the values of the coefficients of multiple correlation for Na, S, and Ca/$R_{Na,\ Si,\ Ca}$/ and for Al, Si, and Ca/$R_{Al,\ Si,\ Ca}$/ for all interface exceed 0.6. That showed that Si and Ca so far as Al and Na could incorporate in such compounds as alumina silicates of sodium and calcium.

Analysis of individual coefficients of multiple correlation, which characterize a bond between two elements in that time, a third element present at a constant level, showed that these coefficients differ in value from the coefficients of pair correlation. This difference is a proof of the interaction of all elements and their interdependence. So, for example, at constant Si, a local coefficient of correlation for Na and Al is equal to 0.26 and at constant Ca—0.96, which is caused by great influence of silicon (Si) on the bond "Na–Al." Almost similar action is rendered by sodium on the bond "Al–Si." This can be seen from comparison of the corresponding local coefficients of correlation. Moreover, the bond between Al and Si is strongly affected by Ca/$R_{Al,Si,Ca}$ = 0.114, in its turn closely connected with bonded Si.

It is worth mentioning that the coefficients of pair correlation for Na and Ca in the case under study are insignificant. However, this is not witnesses the absence of the bond between them, since the individual local coefficient of multiple correlation by alumina is 0.950. Evidently, this bond is considerably affected by aluminum Al, which is much stronger attained by Na.

An interrelation between all elements under study is observed and after interface line from the side of the granule.

The presence of such bond witnesses the appearance of the cement paste/granule interface in the alkali-activated cement concrete of chemical compounds of alkaline, alkali-earth, and mixed alkaline-alkali-earth aluminosilicate composition.

Investigation of specimens of steam-cured alkali-activated cement concrete at the age of 3 years showed that also in this case the compounds containing uniformly/homogeneously interrelated elements, Na, Al, Si, and Ca (all correlation coefficients before the interface line and after it are significant), are present over the ITZ. Moreover, the coefficients of pair correlation for Na and Al/$\zeta_{Na,\ Al}$ = 0.682–0.707/, Na and Si/ $\zeta_{Na,\ Si}$ = 0.796/, and especially for Na and Ca/$\zeta_{\ Na,\ Ca}$ = 0.580–0.620/ at simultaneous increase of common coefficients of multiple correlation significantly increased. A conclusion was made that the aluminum affects the Na-Ca bond and calcium the Na-Al bond. This conclusion is supported by a difference of individual coefficients of correlation between these elements from the coefficients of pair correlation. All this is an evidence that quantities of the compounds of mixed alkaline-alkali-earth alkaline aluminosilicate composition increased in the ITZ. The higher correlation between all elements in time is caused by growth of the hydration products in the ITZ and, hence, densification and strengthening of the interface itself.

The alkali-activated cement concrete with the artificial granular aggregate had a dense structure and was characteristic of high bond strength of the granules with the cement paste. A dense structure of the alkali-activated cement concrete under study, as well as the composition of the hydration products, determine high physical-mechanical properties of such concrete, which, in their turn, determine performance properties.

3.1.2 The processes of structure formation in the ITZ "alkali-activated cement-natural sustainable aggregate"

The structure formation processes in the ITZ of the concretes made using real aggregates were studied on beam specimens (4 × 4 × 16 cm), which were subjected to continuous steam curing for 360 days at temperatures of 38 and 65 ± 3°C.

Micro photos of the ITZs in different concretes made from various cements and aggregates are shown in **Figures 2–7**.

Thin plates for the examination with the help of an electron microscope were cut directly from the beam specimens (4 × 4 × 16 cm).

As it follows from **Figure 2**, significant signs of corrosion in the concretes from traditional (ordinary) Portland cement with crushed basalt rock are seen, the lowest corrosion being in the case with the metakaolin additive (**Figure 2b**).

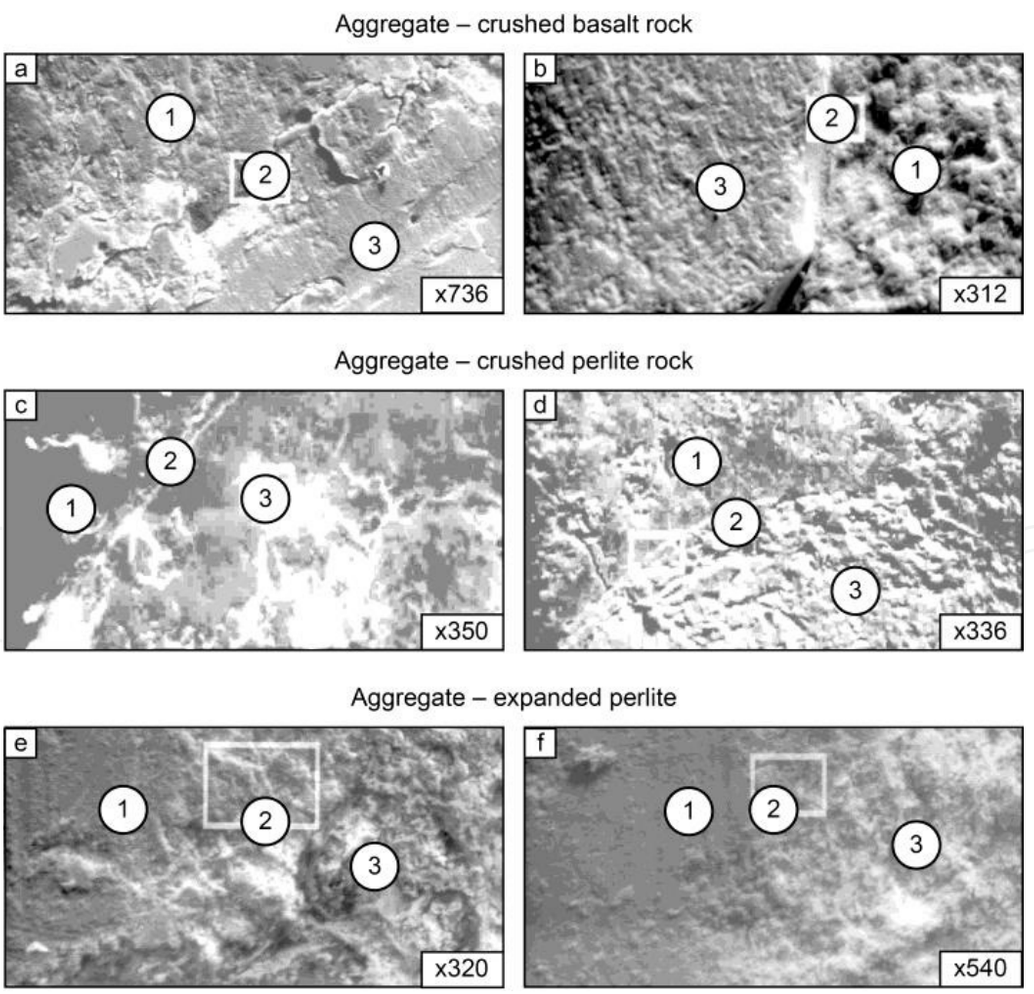

Figure 2.
SEM images of the ITZ concrete—"Portland cement-water-agregate" (a, c, e) without metakaolin additive; (b, d, f) with metakaolin additive; 1, cement stone; 2, ITZ; 3, aggregate. Curing conditions—90 days of steam curing at t = 65°C.

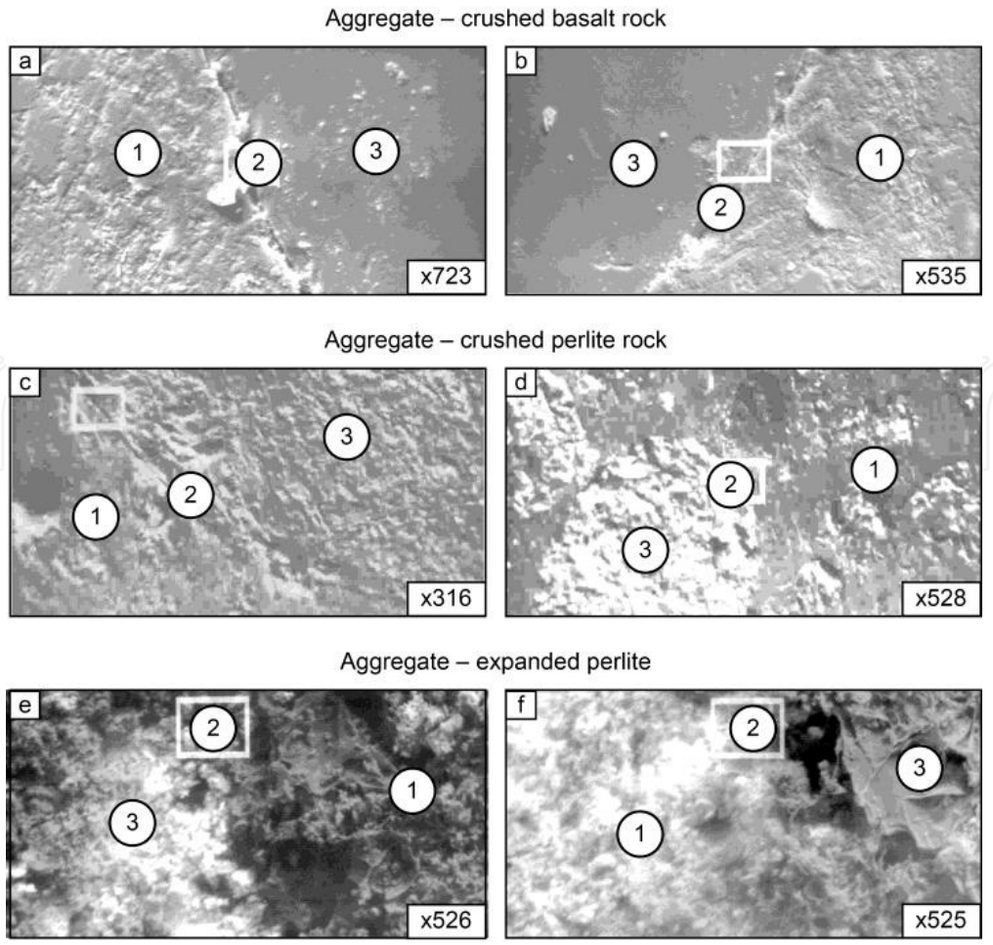

Figure 3.
SEM images of the ITZ concrete—"Portland cement-soluble silicate-agregate" (a, c, e) without metakaolin additive; (b, d, f) with metakaolin additive; 1, cement paste; 2, ITZ; 3, aggregate. Curing conditions—90 days of steam curing at t = 65°C.

The signs of corrosion in the concretes from traditional (ordinary) Portland cement with crushed perlite rock and expanded perlite are, respectively, lower in all cases than those in the case of the crushed basalt rock (**Figure 2e, f**). This can be attributed to the presence in perlite (both expanded and not expanded) of active Al_2O_3 with the glassy phase, which amounts to 90–97%, whereas a quantity of a glassy phase in the crushed basalt rock is only 8–12%. Thus, though a total quantity of Al_2O_3 in the crushed basalt rock and perlite is almost close (14.0% and 12.5–13.2%, respectively) (**Table 3**), active Al_2O_3 is contained in the perlite in much higher amounts. Moreover, in compliance with [4, 41], it may be allowed that a part of the products of corrosion depose in a pore space of the perlite, thus eliminating a little bit their deleterious action.

The compositions of the alkali-activated Portland cement with high-modulus soluble silicate as alkaline activator are given in **Figure 3**. Metakaolin was used as a modifying additive. Analysis of the micro photos showed that the hydration reaction products are mostly observed in the composition with the crushed basalt rock without additive (**Figure 3a**). The additive of metakaolin improves the picture. The ITZ became sharp and clear (**Figure 3b**).

In the compositions with the crushed perlite rock and expanded perlite using alkali-activated Portland cement with soluble silicate some signs of corrosion are present in the ITZ in the additive-free compositions and are practically absent in the compositions with the metakaolin additive (**Figure 3c–f**).

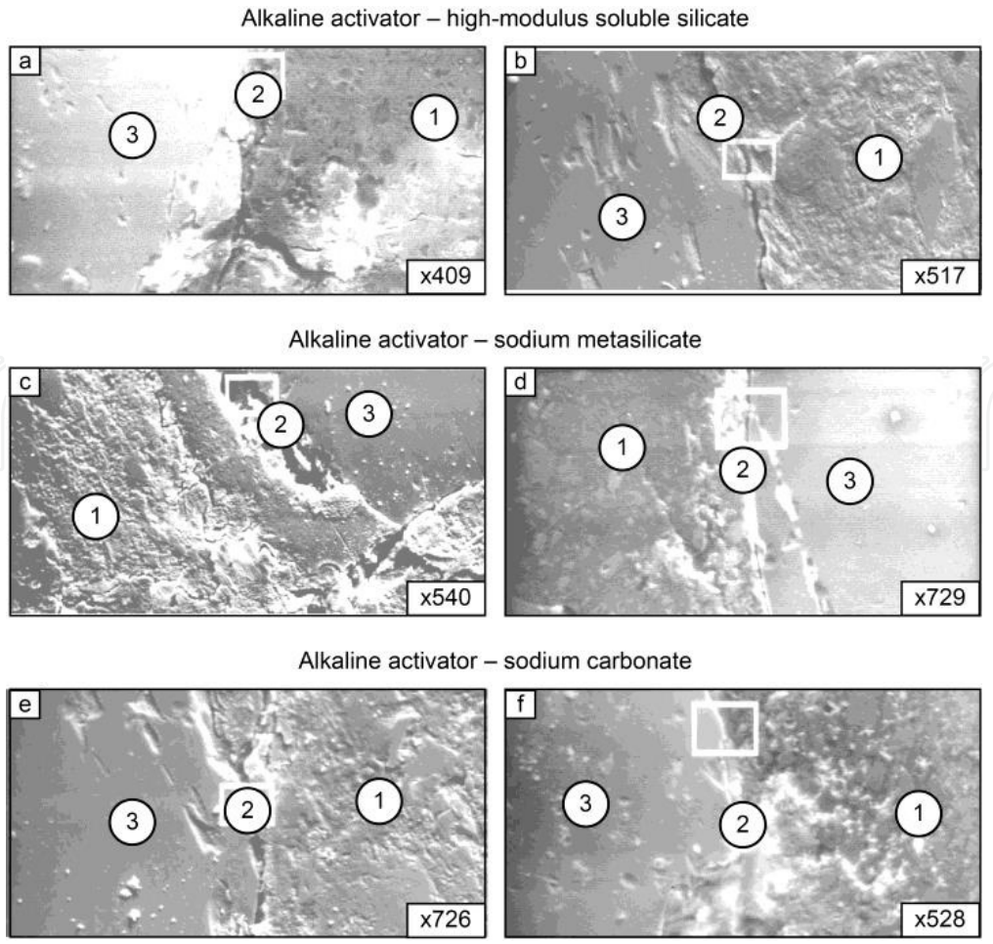

Figure 4.
SEM images of the ITZ concrete—"GBFS-alkaline component-basalt rock" (a, c, e) without metakaolin additive; (b, d, f) with metakaolin additive; 1, cement paste; 2, ITZ; 3, aggregate. Curing conditions—90 days of steam curing at t = 65°C.

The nature of flow of corrosion processes in the alkali-activated slag compositions with high-modulus soluble silicate is mostly similar to the compositions using alkali-activated Portland cement (**Figure 4a, b**).

Reducing of silicate modulus of soluble silicate down to Ms = 1 (sodium metasilicate) and the use of solution of sodium carbonate (**Figure 4a, e**) leads to decreasing of corrosion products in the ITZ in the additive-free compositions compared to compositions using high-modulus soluble silicate (**Figure 4a**). The metakaolin additive influenced positively on slowing of corrosion processes in the ITZ (**Figure 4b, d, f**).

The influence of the curing conditions of the specimens on the development of the corrosion processes is shown in **Figures 5** and **6**, where results of observation of compositions using traditional (ordinary) and alkali-activated Portland cement with crushed basalt rock are given, which cured for 90 days at t = 20, 38, and 65°C and RH =100%.

It is shown that in this period at t = 20°C, there are practically no any signs of corrosion in the ITZ "cement stone-aggregate" in both compositions, both with and without the metakaolin additive, being fixed (**Figure 5a, b**). ITZ в additive-free compositions at t = 38°C (**Figures 5c, 6c**) are a little bit less expressed and even less at t = 65°C (**Figures 5e, 6e**). The presence of the kaolin makes the ITZ more clearly expressed (**Figures 5d, f** and **6d, f**).

The study on microhardness of the ITZ in the concretes with crushed basalt rock showed that the metakaolin additive within the alkali-activated cements intensifies constructive corrosion (**Figure 7**).

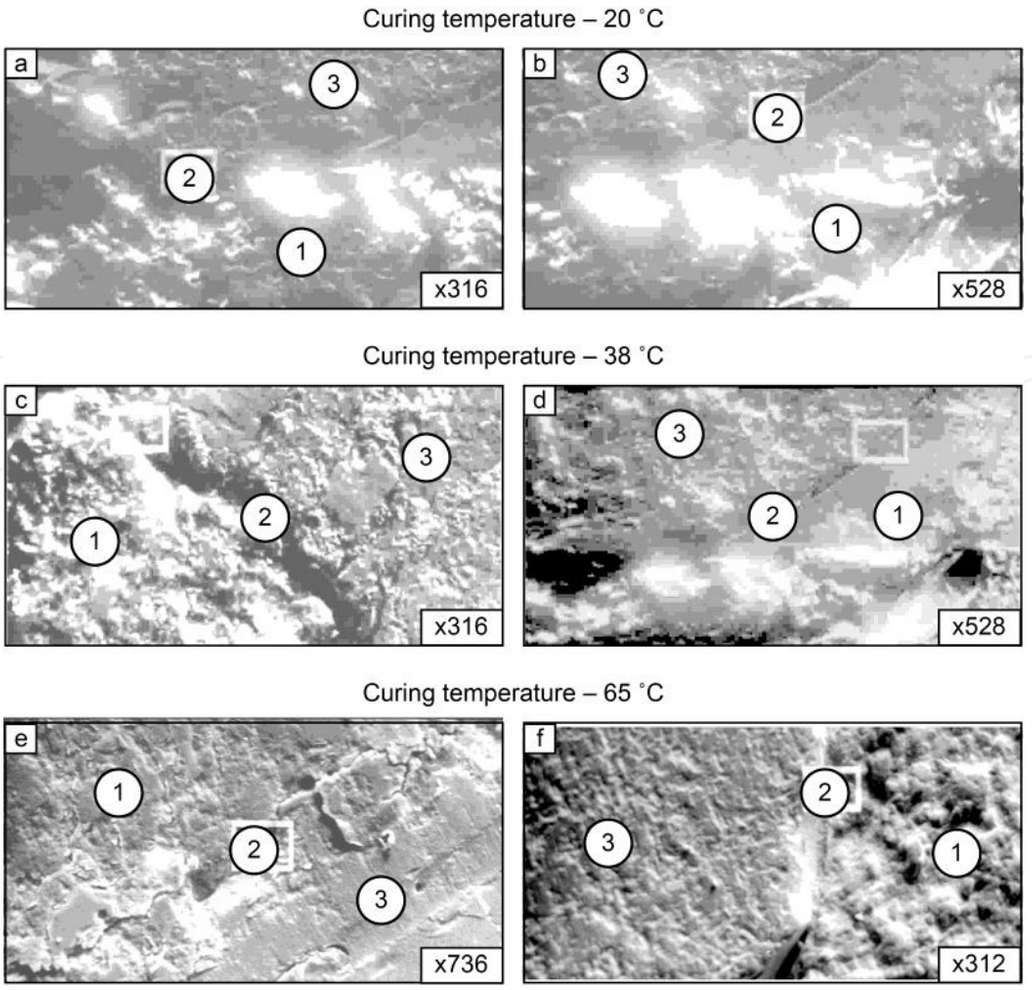

Figure 5.
SEM images of the ITZ concrete—"Portland cement-water-crushed basalt rock" (a, c, e) without metakaolin additive; (b, d, f) with metakaolin additive; 1, cement paste; 2, ITZ; 3, aggregate. Curing conditions at t = 20, 38, 65°C 90 days after steam curing.

Thus, taking into account micro photos of the cement paste/alkali-susceptible aggregate ITZ, the following conclusions can be drawn:

- At t = 20°C at an age of 90 days, all concrete specimens under study, not depending upon a cement type and kind of aggregate, showed *clear presence* of destructive processes in the ITZ.

- At t = 38°C at an age of 90 days in additive-free compositions, except for those with perlite, in most cases there are fixed disturbance of sharpness and integrity of the ITZ. The addition of the metakaolin to the traditional (ordinary) Portland cement and alkali-activated cements reduces a quantity of undesirable reaction products in the ITZ.

At the temperature t = 65°C at an age of 90 days, disturbance of the ITZ is much more clearly expressed than that at t = 38°C, chiefly, in the concretes from cement without additives. Exceptions are the concretes with perlite, where the products of corrosion, probably, could distribute in a pore space of the aggregate and, above all, perlites are represented, chiefly, by a glassy phase with rather high contents of active alumina, which can bind rather effectively free alkalis, reducing, in this way, a risk of active silica-aggregate reaction. The metakaolin additive in all cases influences positively on reducing deposits of the products of corrosion in the ITZ.

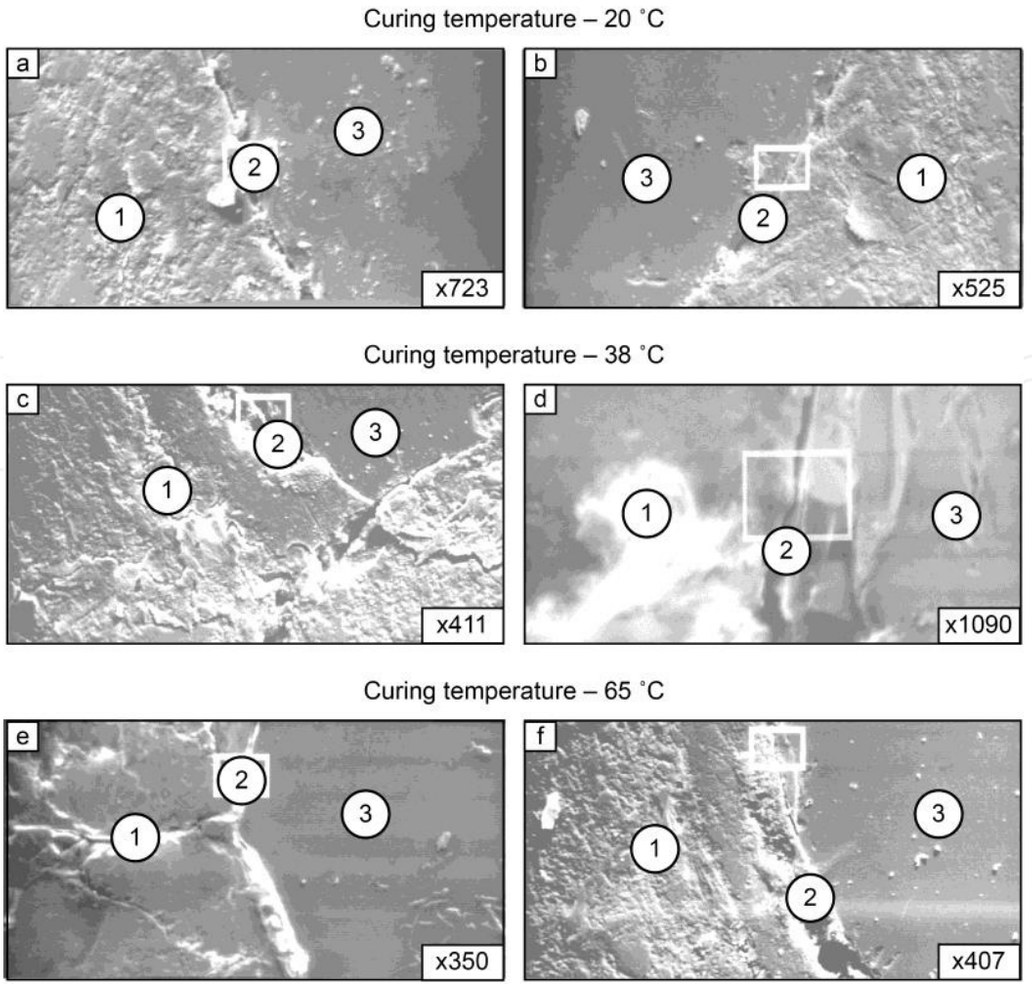

Figure 6.
Micro photos of the ITZ concrete—"Portland cement + soluble glass-basalt rock" (a, c, e) without metakaolin additive; (b, d, f) with metakaolin additive; 1, cement paste; 2, ITZ; 3, aggregate. Curing conditions at t = 20, 38, 65°C 90 days after steam curing.

XRD patterns of the specimens, modeling the cement stone/alkali-susceptible aggregate ITZ, are shown in **Figures 8–11**.

Thus, in **Figure 8** the diffraction characteristic of composition on the basis of basalt and Portland cement (ordinary and alkali-activated) after their hardening in the conditions of continuous steam curing for 360 days is represented.

Corresponding to the XRD analysis data, a phase composition of the hydrated dispersions based on ordinary Portland cement and basalt (**Figure 8**, curve 2), modeling the ITZ, is represented, chiefly, by the following hydrate new formations: high-basic calcium silicate hydrates of the C_6S_3H (d = 0.335–0.284–0.246–0.237–0.225–0.180 nm), C_2SH (d = 0.284–0.270–0.246–0.190–0.180 nm) types, and low-basic phases of the $C_3S_2H_3$ (d = 0.56–0.284–0.184 nm) type. The presence of $Ca(OH)_2$ (d = 0.487–0.311–0.261–0.193–0.180 nm) and $CaCO_3$ (d = 0.303–0.229–0.21–0.193–0.188 nm) also was fixed. Also there are set weak lines of the C_2AH_4 (d = 7.17–0.376–0.266–0.258–0.246 nm) type. It is well-known that via the presence of chemically active silica and alkalis, in this case Ca(OH), which is present in the pores of the hardened concrete, a deleterious reaction "alkali-silicic acid" takes place actively with formation of alkaline metal silicate gel in the aggregate/cement stone ITZ. XRD analysis is not fixing X-ray amorphous phase of calcium silicate gel, which may be forming in the ITZ and weakening it, but taking into elemental distribution in the ITZ and extremely high expansion deformations of composite materials with basalt (up to 2.15 mm/m), such possibility exists and mostly is confirmed by the higher contents of Ca and Si in the ITZ.

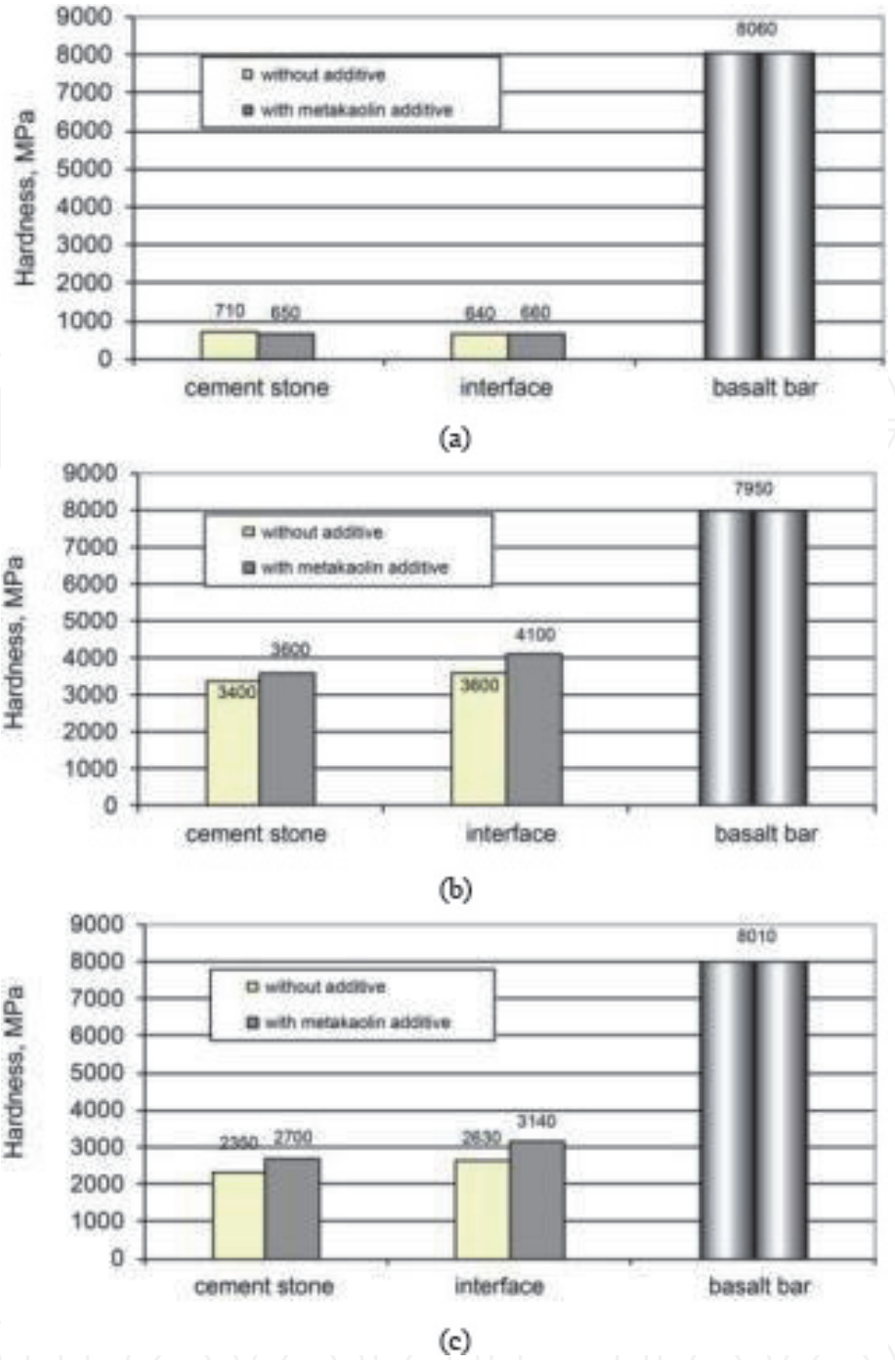

Figure 7.
Hardness of the ITZ "cement stone-basalt" (a) cement stone + water; (b) cement stone + soluble silicate; (c) GBFS + soluble silicate. Curing conditions—60 days of continuous steam curing at t = 65°C.

Use in the composition with basalt of the alkali-activated Portland cement leads to the changes in diffraction picture of the ITZ model (**Figure 8**, curve 3). Thus, hydration depth of Portland cement is rising, resulting in reducing intensiveness of the diffraction lines. Transformation of phase formation processes took place in the direct of formation of low-basic silicate hydrates of calcium CSH(I) (d = 0.283–0.270–0.247–0.179 nm) type and tobermorite (d = 0.560–0.307–0.299–0.283–0.227–0.208–0.183 nm). The reflexes of $Ca(OH)_2$ are totally absent.

In the ITZ silica, content reduces rapidly; at the same time, the quantity of aluminum and sodium is rising. Thus it is possible to make a conclusion about synthesis in the ITZ of sodium and mixed sodium-calcium alumina silicates, confirming by the results of X-ray diffractogram analysis (**Figure 9**, curve 2). Thus,

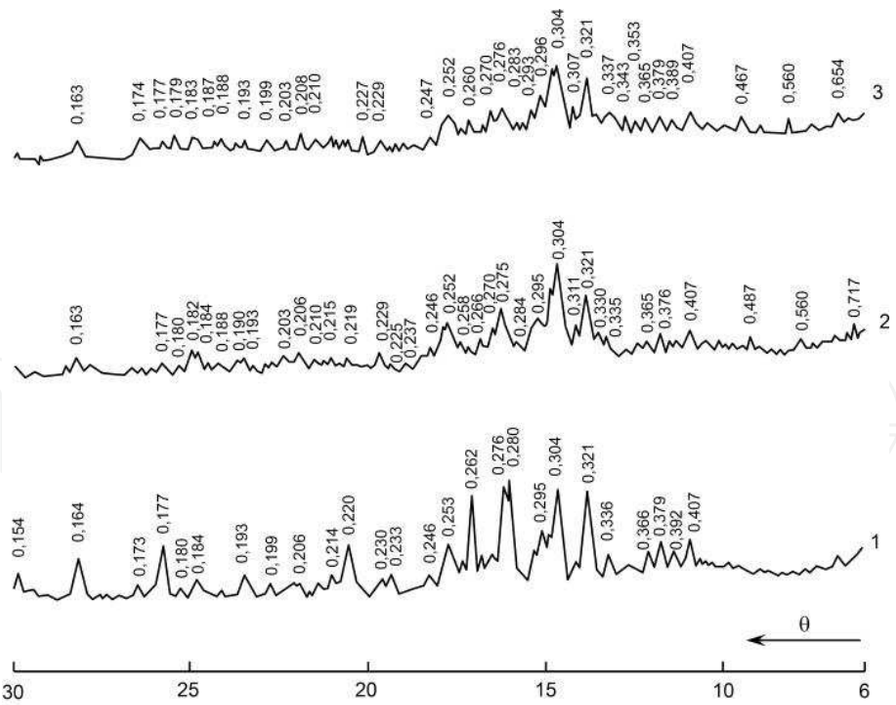

Figure 8.
XRD patterns of the ITZ of model systems: (1) "Portland cement-basalt"; (2) "Portland cement-basalt-water"; (3) "Portland cement-basalt-soluble silicate." Curing conditions—360 days at t = 65 ± 3°C and RH = 100%.

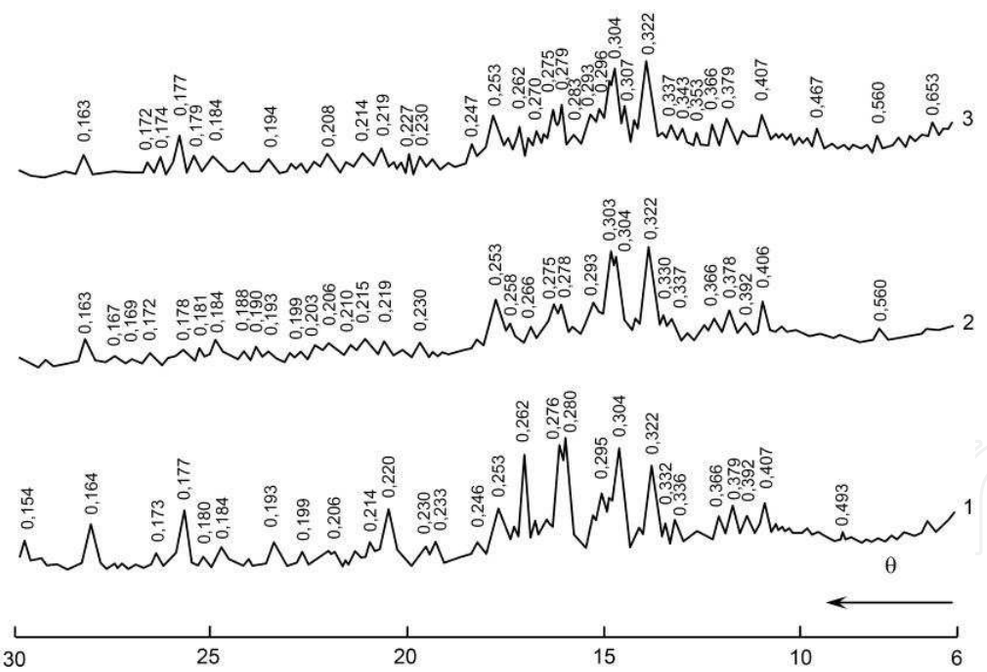

Figure 9.
XRD patterns of the ITZ of model systems: (1) "Portland cement-metakaolin-basalt"; (2) "Portland cement-metakaolin-basalt-water"; (3) "Portland cement-metakaolin-basalt-soluble silicate." Curing conditions—360 days at t = 65 ± 3°C and RH = 100%.

at curve 3 appears lines of the $Na_2O{\cdot}Al_2O_3{\cdot}4SiO_2{\cdot}2H_2O$ (d = 0.56–0.343–0.293–0.252–0.174 nm) and $2Na_2O{\cdot}2CaO{\cdot}5Al_2O_3{\cdot}10SiO_2{\cdot}10H_2O$ (d = 0.654–0.467–0.353–0.283–0.270 nm) phases.

Introducing of the metakaolin additive to ordinary Portland cement mixes with water significantly not changing diffraction picture (**Figure 9**, curve 3). However, as it seems from **Figure 9**, in the ITZ significantly reducing content of Ca, and also

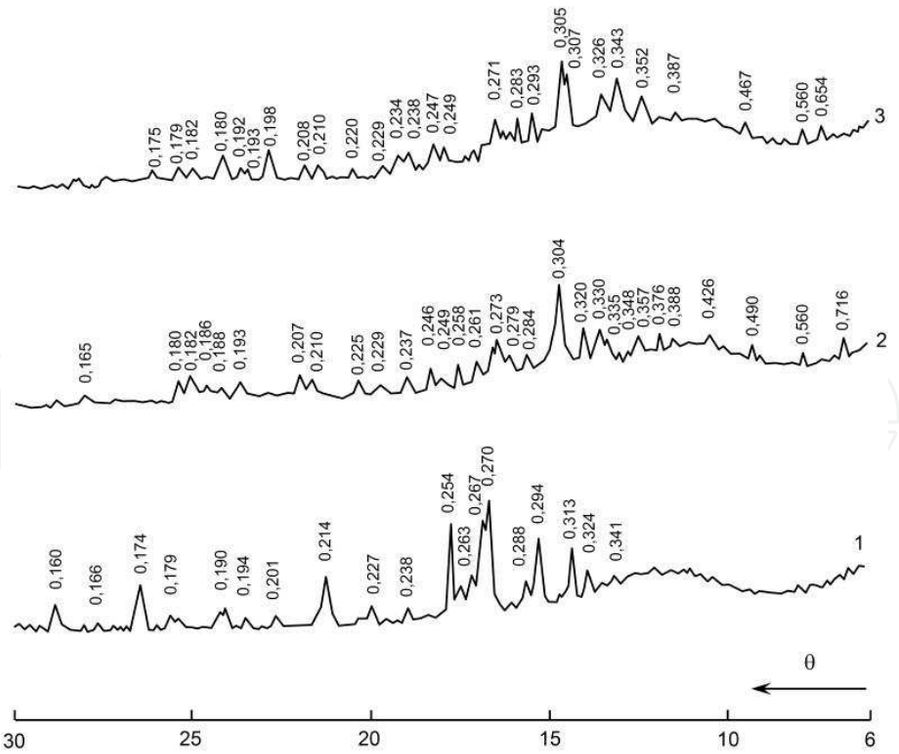

Figure 10.
XRD patterns of the ITZ of model systems: (1) "Portland cement-perlite"; (2) "Portland cement-perlite-water"; (3) "Portland cement-perlite-soluble silicate." Curing conditions—360 days at t = 65 ± 3°C and RH = 100%.

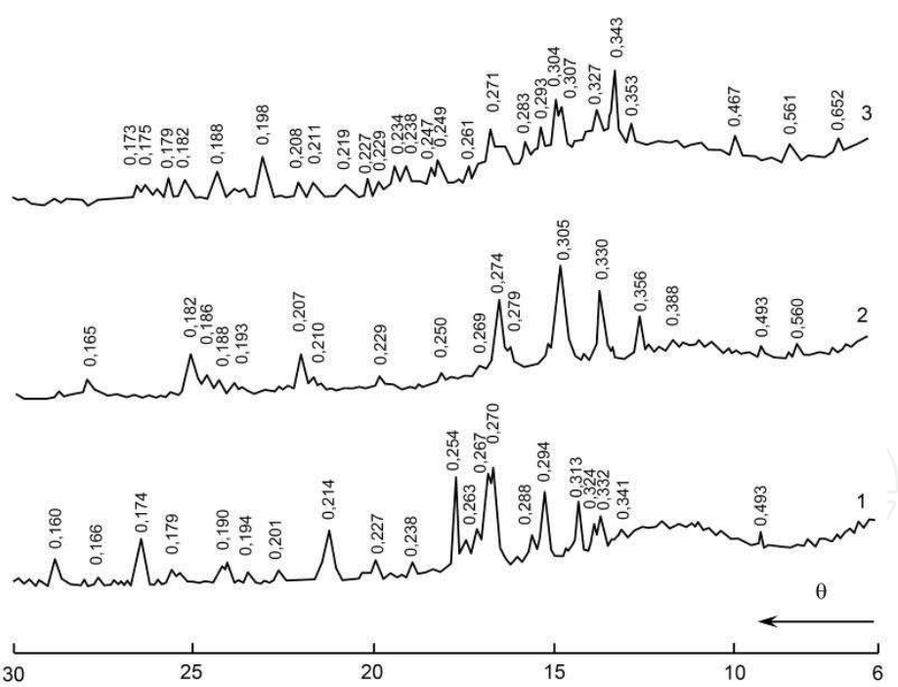

Figure 11.
XRD patterns of the ITZ of model systems: (1) "Portland cement-metakaolin-perlite"; (2) "Portland cement-water-metakaolin-perlite"; (3) "Portland cement-soluble silicate + metakaolin-perlite." Curing conditions—360 days at t = 65 ± 3°C and RH = 100%.

hydroxide ions, significantly reduces risk of corrosion processes in the ITZ in destructive form. This correlates well with the data in [9], corresponding to which the presence of active alumina in the Portland cement stone significantly reduces alkali concentration in the pore space of Portland cement stone.

The last consideration is absolutely confirmed in the case of replacement of ordinary Portland cement by alkali-activated Portland cement with the metakaolin additive. Thus,

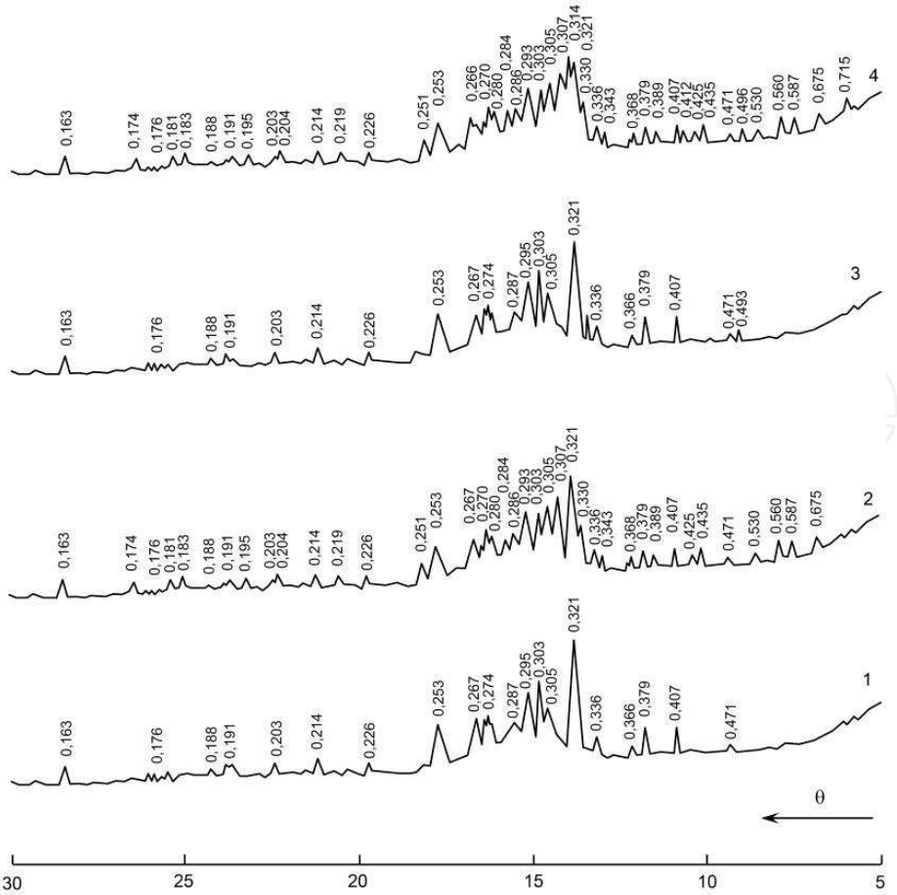

Figure 12.
XRD patterns of the ITZ of model systems: (1) "GBFS-basalt"; (2) "GBFS-soluble silicate-basalt"; (3) "GBFS-metakaolin-basalt"; (4) "GBFS-soluble silicate-metakaolin-basalt." Curing conditions—360 days at t = 65 ± 3°C and RH = 100%.

according to **Figure 9**, curve 2, hydration of Portland cement deepens, forming fine-grained crystalline structure. The zeolite-like new formations—$Na_2O{\cdot}Al_2O_3{\cdot}4SiO_2{\cdot}2H_2O$ (d = 0.561–0.343–0.293–0.251–0.174 nm), $Na_2O{\cdot}Al_2O_3{\cdot}3SiO_2{\cdot}2H_2O$ (d = 6.53–5.87–4.36–2.86–2.19 nm) and $2Na_2O{\cdot}2CaO{\cdot}5Al_2O_3{\cdot}10SiO_2{\cdot}10H_2O$ (d = 0.654–0.467–0.353–0.285–0.269 nm)—are synthesizing in the ITZ, which is proven by increasing of Al and Na and reducing of Ca content in the ITZ.

Use of alkali-activated slag cement is characterized by the more active synthesis in the alkali-susceptible aggregate/cement stone ITZ of the low-basic hydrate new formations as silicate, so as alumina silicate composition (**Figure 12**). This process becomes greatly active exactly in the presence of metakaolin additive. Thus, in the model system of the ITZ "alkali-activated slag cement stone-basalt aggregate," there are fixed zeolite-like new formations of the $Na_2O{\cdot}Al_2O_3{\cdot}4SiO_2{\cdot}2H_2O$ (d = 0.56–0.343–0.293–0.252–0.174 nm) and $Na_2O{\cdot}Al_2O_3{\cdot}3SiO_2{\cdot}2H_2O$ (d = 0.653–0.587–0.436–0.286–0.219 nm) types as well as low-basic silicate hydrates CSH(I) (d = 0.530–0.304–0.28–0.181 nm) and xonotlite $6CaO{\cdot}6SiO_2{\cdot}H_2O$ (d = 0.425–0.389–0.368–0.330–0.307–0.284–0.270–0.204–0.195 nm). That is confirmed by analysis of the elemental distribution in the ITZ of the taken composition (**Figure 12**). Thus, in the presence of metakaolin additive, reflexes of the mentioned above new formations became sharper. Moreover, there is fixed new formation $2Na_2O{\cdot}2CaO{\cdot}3Al_2O_3{\cdot}10SiO_2{\cdot}12H_2O$ type (d = 0.715–0.495–0.412–0.314–0.266 nm), which is also classified as zeolites (**Figure 12**, curve 4).

Metakaolin additive reduces Ca content not only in the ITZ but also in cement stone, showing possibility of synthesis of the aluminosilicate hydrates of mixed sodium-calcium composition not only in the ITZ but in the cement matrix as well.

It is known that there exist no absolutely inert aggregates. All aggregates more or less react to the cement stone. But in some cases in the ITZ, destructive processes took place, with "negative effect of corrosion," meaning with gradual destruction, and in other cases—structure formation processes with the "positive effect of corrosion," meaning without destruction and moreover with improvement state of the ITZ.

In the alkali-activated cement concretes, especially cements containing the metakaolin additive, at the surface of the aggregates appears a dense film of new formation mostly represented by alumina silicate hydrate composition, which prevents further admission of new portions of alkalis to the aggregate. Thus a way, due to the partial corrosion of aggregate at the initial stages, on its surface it is forming protective dense and impermeable capsule.

On the contrary to alkali-activated cement concretes, in ordinary Portland cement concretes, gel-like new formations in the ITZ act as semipermeable films. That means that alkalis are able to easy penetrate through new formations to aggregate grain and new products of corrosion are accumulating under that film, increasing osmotic pressure and leading to the degradation of ITZ and destruction of concrete in general.

Thus, in the result of provided studies, the effectiveness of introduction into the alkali-activated cement compositions with alkali-susceptible aggregates of active alumina represented by metakaolin was proven, which makes it possible to bond extra alkalis effectively and regulate structure formation processes in the cement stone/alkali-susceptible aggregate ITZ, using partial surface corrosion of the aggregate for synthesis in the interface of the zeolite-like hydrate phases.

3.2 Physical-mechanical properties of concretes

3.2.1 Concrete mixture "Portland cement + water"

The results of determination of compressive and bending strengths of the concrete specimens made using the Portland cement as well as their autogenous deformations are given in **Table 4**.

Taking into account data from the **Table 4**, depending upon curing conditions of compositions and using as a criteria corrosion in the ITZ and the admissible values of expansion of the specimens not exceeding 1 mm/m (0.1%) [42] with simultaneous consideration of their strength characteristics, the following conclusions can be drawn.

3.2.1.1 Curing conditions: t = 20 °C, RH = 100%

Curing of Portland cement specimens at t = 20°C more or less considerable corrosion in all control ages (28–180 days) for all composition is not fixed, not depending upon composition of the specimens. Strength (compressive and bending) characteristics of the specimens in these curing conditions at the given ages tended to increase.

Reducing of shrinkage in the concretes made with basalt aggregates at an age of 90 and 180 days compared to that in 28-day age is set as insignificant, which witnesses the beginning of a reverse process, meaning free development of corrosion processes in the ITZ of the concretes made using aggregates.

The metakaolin additive considerably decreased autogenous deformations of shrinkage of the Portland cement containing specimens compared to additive-free compositions, losing at the same time strength of the specimens compared to additive-free compositions.

L/S[1]	Additive	Temperature, °C	Strength compressive/ bending, MPa, age, days			Shrinkage (expansion) deformations, mm/m, age, days[2]		
			28	90	180	28	90	180
"Portland cement + water + crushed basalt rock"								
36	—	20	70.1 / 7.1	76.0 / 9.3	77.7 / 11.1	−0.50	−0.44	−0.40
		65	75.9 / 9.4	72.8 / 9.2	70.9 / 9.0	+0.15	+0.69	+1.08
38	Metakaolin	20	64.2 / 6.8	75.2 / 6.7	76.6 / 7.0	−0.41	−0.30	−0.23
		65	69.0 / 7.2	56.3 / 6.9	52.0 / 6.7	+0.10	+0.52	+0.74
"Portland cement + water + chopped waste of basalt fiber production"								
45	—	20	39.8 / 10.2	40.8 / 12.2	45.9 / 11.1	−0.46	−0.41	−0.30
		65	52.7 / 11.9	50.3 / 7.8	48.4 / 7.9	+0.11	+0.55	+0.99
48	Metakaolin	20	45.4 / 9.8	50.8 / 12.1	52.2 / 11.6	−0.38	−0.34	−0.20
		65	46.4 / 8.9	40.0 / 7.9	38.8 / 7.2	+0.13	+0.48	+0.59
"Portland cement + water + crushed perlite rock"								
51	—	20	68.2 / 7.0	76.0 / 9.0	—	−0.51	−0.56	—
		65	73.8 / 9.3	72.8 / 9.0	—	+0.11	+0.23	—
53	Metakaolin	20	66.4 / 6.8	73.1 / 6.9	—	−0.48	−0.49	—
		65	53.0 / 7.1	54.3 / 6.9	—	+0.07	+0.18	—
"Portland cement + water + expanded perlite"								
37	—	20	31.0 / 1.4	34.1 / 2.0	—	−0.65	−0.70	—
		65	36.4 / 2.5	37.2 / 1.9	—	−0.41	−0.35	—
38	Metakaolin	20	29.2 / 2.0	35.0 / 2.3	—	−0.53	−0.59	—
		65	36.1 / 2.4	37.7 / 2.3	—	−0.29	−0.27	—

[1] *L/S, liquid-to-cement ratio.*
[2] *A minus sign (−), shrinkage; plus sign (+), expansion of the specimens in relation to a basic measurement.*

Table 4.
Strength characteristics and autogenous deformations of the concretes using cement system "OPC + water" vs. curing conditions and concrete mixture design.

3.2.1.2 Curing conditions: t = 65°C, RH = 100%

The most considerable changes, so as it was expected, were found in the structure of the ITZ of the specimens made using Portland cement curing at t = 65°C. So,

L/S[1]	Additive	Temperature °C	Strength compressive/ bending, MPa, age, days			Shrinkage (expansion) deformations, mm/m, age, days[2]		
			28	90	180	28	90	180
"Portland cement + soluble silicate + crushed basalt rock"								
354	—	20	59.8 / 5.1	76.0 / 4.8	128.2 / 6.4	−0.63	−0.55	−0.51
		65	115.5 / 7.0	128.1 / 6.5	132.0 / 6.4	+0.18	+0.70	+0.81
354	Metakaolin	20	92.1 / 5.0	106.0 / 5.3	117.7 / 6.3	−0.61	−0.49	−0.36
		65	111.1 / 7.1	126.9 / 7.7	130.0 / 7.3	+0.09	+0.45	+0.48
"Portland cement + soluble silicate + chopped off-size basalt fibers"								
454	—	20	44.0 / 8.9	69.6 / 8.7	81.9 / 10.9	−0.47	−0.41	−0.38
		65	93.9 / 10.3	93.5 / 11.4	88.7 / 9.1	+0.12	+0.63	+0.72
454	Metakaolin	20	62.4 / 5.8	73.3 / 6.9	88.0 / 9.3	−0.58	−0.60	−0.57
		65	90.9 / 11.2	103.8 / 12.0	109.8 / 11.8	+0.10	+0.44	+0.46
"Portland cement + high-modulus soluble silicate + crushed perlite rock"								
51	—	20	75.2 / 6.1	79.3 / 5.9	—	−1.10	−1.15	—
		65	88.0 / 6.8	91.0 / 7.4	—	+0.16	+0.18	—
52	Metakaolin	20	73.7 / 6.2	76.1 / 6.2	—	−0.64	−0.67	—
		65	88.9 / 7.1	93.0 / 7.3	—	−0.04	+0.10	—
"Portland cement + high-modulus soluble silicate + expanded perlite"								
36	—	20	39.9 / 2.0	42.3 / 2.3	—	−1.22	−1.26	—
		65	44.4 / 2.7	45.5 / 2.5	—	−0.68	−0.66	—
37	Metakaolin	20	37.7 / 2.1	43.5 / 2.2	—	−0.79	−0.83	—
		65	44.2 / 2.7	47.0 / 2.8	—	−0.38	−0.34	—

[1] *L/S, liquid-to-cement ratio.*
[2] *A minus sign (−), shrinkage; plus sign (+), expansion.*

Table 5.
Strength characteristics and autogenous deformations of the concretes using cement system "OPC + soluble glass" vs. curing conditions and concrete mixture design.

at an age of 180 days in the concrete specimens with crushed basalt rock without admixture, extremely high (dangerous) values of expansion—1.08–1.17 mm/m—were found, reflexing in some drop of strength characteristics, both compressive

and bending, of the specimens compared to those concretes of 28-day age at t = 65°C. The addition of the metakaolin additive allowed to reduce the expansion values at an age of 180 days to the safer level—0.74 mm/m.

L/S[1]	Additive	Temperature, °C	Strength compressive/ bending, MPa, age, days			Shrinkage (expansion) deformations, mm/m, age, days[2]		
			28	90	180	28	90	180
"GBFS + high-modulus soluble silicate + crushed basalt stone"								
0.36	—	20	61.7 / 6.1	78.0 / 6.0	108.0 / 7.2	−1.21	−1.01	−0.78
		65	103.3 / 8.0	116.0 / 7.4	120.1 / 7.0	+0.58	+0.88	+0.91
0.36	Metakaolin	20	81.3 / 6.2	95.0 / 6.3	103.7 / 6.6	−1.19	−0.85	−0.73
		65	100.3 / 8.8	115.0 / 8.2	119.8 / 9.0	+0.44	+0.46	+0.47
"GBFS + high-modulus soluble silicate + glassy waste product of basalt fibers production"								
0.45	—	20	92.0 / 10.7	94.9 / 10.9	95.0 / 11.1	−0.83	−0.86	−0.82
		65	102.0 / 12.0	100.3 / 9.0	97.2 / 8.9	+0.63	+0.86	+0.87
0.45	Metakaolin	20	78.0 / 12.1	88.7 / 11.9	99.8 / 12.0	−0.66	−0.63	−0.65
		65	108.0 / 10.8	111.0 / 11.3	115.2 / 11.2	+0.41	+0.44	+0.45
"GBFS + high-modulus soluble silicate + crushed perlite rock"								
0.50	—	20	81.0 / 5.9	85.0 / 5.8	—	−1.17	−1.20	—
		65	94.8 / 6.9	97.0 / 7.3	—	+0.12	+0.15	—
0.51	Metakaolin	20	79.8 / 6.0	82.0 / 6.1	—	−0.71	−0.73	—
		65	95.2 / 7.2	98.9 / 7.2	—	−0.13	+0.09	—
"GBFS + high-modulus soluble silicate + expanded perlite"								
0.35	—	20	37.0 / 1.7	40.2 / 2.2	—	−1.33	−1.40	—
		65	42.4 / 2.5	43.3 / 2.4	—	−0.75	−0.67	—
0.36	Metakaolin	20	35.4 / 2.0	40.3 / 2.3	—	−0.87	−0.89	—
		65	42.1 / 2.1	44.8 / 2.5	—	−0.37	−0.34	—

[1] *L/S, liquid-to-cement ratio.*
[2] *A minus sign (−), shrinkage; plus sign (+), expansion.*

Table 6.
Strength characteristics and autogenous deformations of the concretes using cement system "GGBS + soluble glass" vs. curing conditions and concrete mixture design.

3.2.2 Concrete mixture "Portland cement + soluble silicate"

The results of determination of compressive and bending strengths of the concrete specimens made using the alkali-activated Portland cement as well as their autogenous deformations are given in **Table 5**. The characteristics are varied depending on composition and curing conditions.

3.2.3 Concrete mixture "GBFS + soluble silicate"

The results of determination of compressive and bending strengths of the concrete specimens made using the alkali-activated slag cement with high-modulus soluble silicate, sodium metasilicate, and sodium carbonate as alkaline activators as well as their autogenous deformations are given in **Table 6**. The characteristics are varied depending on composition and curing conditions.

The development of shrinkage/expansion deformations of the concrete containing "GBFS + soluble silicate" as cement and crushed basalt rock as aggregate suggested to conclude that at almost complete similarity of regularities, they differ from that made using the alkali-activated Portland cement only in absolute values of characteristics—those are in some cases a little bit higher. A value of maximal expansion of the concrete containing "GBFS + soluble silicate" as cement and crushed basalt rock as aggregate within the ranges of experiment was 0.45–0.91 mm/m (**Table 6**) and those in the case of the alkali-activated Portland cement —0.46–0.81 mm/m (**Table 5**).

A character of strength gain of all compositions for all temperature regimes is stable and without any drops (**Table 6**).

4. Conclusions

The processes of structure formation in the ITZ "alkali-activated cement-artificial aggregate" are studied. It is set that the interface between them practically disappears, which indicates about penetration of the elements and blurring the border between the cement stone and the aggregate.

It is established that the positive result of the processes of such interaction of the substances of cement elements and aggregate is the formation of alkaline and alkaline-alkali-earth alumina silicate hydrates—analogs of natural zeolites, transforming a destructive process of concrete corrosion into the constructive.

Comparative studies of the processes of the structure formation of the ITZ in the alkali-activated cement concretes with different alkali-susceptible aggregates confirmed that Al_2O_3 plays a determining role in these constructive processes.

It is shown that the addition of the metakaolin additive as an Al_2O_3-containing additive provides inhibition of alkaline corrosion processes, which is confirmed by long-term testing of strength characteristics and deformation (shrinkage/expansion) of concretes using different alkali-activated cements and alkali-susceptible natural aggregates.

Author details

Pavel Krivenko*, Oleh Petropavlovskyi, Oleksandr Kovalchuk and Oleksandr Gelevera
Scientific Research Institute for Binders and Materials, Kyiv National University of Construction and Architecture, Kyiv, Ukraine

*Address all correspondence to: pavlo.kryvenko@gmail.com

IntechOpen

References

[1] Stark J, Wicht B. Alkali-Kieselsäure-Reaktion. Weimar: Verlag; 2008

[2] Krivenko PV. Peculiarity of formation of the contact zone (slag alkaline cement mineral wool). In: Second International Symposium on Cement and Concrete Technology; Istanbul, Turkey; 2000. pp. 553-559

[3] Schäfer E. Einfluss der reaktionen verschiedener zementhauptbestandteile auf den alkalihaushalt der porenlösung des zementsteins [Diss]. Verlag Nicht Ermittelbar; 2006

[4] Ramlochan T, Thomas M, Gruber KA. The effect of metakaolin on alkali–silica reaction in concrete. Cement and Concrete Research. 2000; **30**(3):339-344

[5] Krivenko PV. Structure-forming processes in the interfacial transition zone "alkali activated slag cement–aggregate". Tsement, Leningrad, USSR; 1991;**11–13**:64-70

[6] Stark J, Wicht B. Dauerhaftigkeit von Beton. Basel, Switzerland: Birkhauser Verlag; 2001

[7] Visser JHM. Fundamentals of alkali-silica gel formation and swelling: Condensation under influence of dissolved salts. Cement and Concrete Research. 2018;**105**:18-30. DOI: 10.1016/j.cemconres.2017.11.006

[8] Lindgård J, Andiç-Çakir Ö, Fernandes I, Rønning TF, Thomas MDA. Alkali-silica reactions (ASR): Literature review on parameters influencing laboratory performance testing. Cement and Concrete Research. 2012;**42**:223-243. DOI: 10.1016/j.cemconres.2011.10.004

[9] Fournier B, Bérubé M-A. Alkali-aggregate reaction in concrete: A review of basic concepts and engineering implications. Canadian Journal of Civil Engineering. 2000;**27**:167-191. DOI: 10.1139/l99-072

[10] Gifford PM, Gillott JE. Alkali-silica reaction (ASR) and alkali-carbonate reaction (ACR) in activated blast furnace slag cement (ABFSC) concrete. Cement and Concrete Research. 1996; **26**:21-26

[11] Pignatelli R, Comi C, Monteiro PJM. A coupled mechanical and chemical damage model for concrete affected by alkali-silica reaction. Cement and Concrete Research. 2013;**53**:196-210. DOI: 10.1016/j.cemconres.2013.06.011

[12] Poyet S, Sellier A, Capra B, Foray G, Torrenti JM, Cognon H, et al. Chemical modelling of alkali silica reaction: Influence of the reactive aggregate size distribution. Materials and Structures. 2007;**40**:229-239. DOI: 10.1617/s11527-006-9139-3

[13] Dunant CF, Scrivener KL. Micro-mechanical modelling of alkali-silica-reaction-induced degradation using the AMIE framework. Cement and Concrete Research. 2010;**40**: 517-525. DOI: 10.1016/j.cemconres.2009.07.024

[14] Esposito R, Hendriks MAN. Literature review of modelling approaches for ASR in concrete: A new perspective. European Journal of Environmental and Civil Engineering. 2017;**8189**:1-21. DOI: 10.1080/19648189.2017.1347068

[15] Multon S, Sellier A, Cyr M. Chemo-mechanical modeling for prediction of alkali silica reaction (ASR) expansion. Cement and Concrete Research. 2009; **39**:490-500. DOI: 10.1016/j.cemconres.2009.03.007

[16] Li K, Coussy O. Concrete ASR degradation: From material modeling to

structure assessment. Concrete Science and Engineering. 2002;**4**:35-46. Available from: https://www.researchgate.net/publication/281155830

[17] Gartiser S, Rudolf R. Machbarkeitsstudie zur Formulierung von Anforderungen fuer ein neues Umweltzeichen fuer Enteisungsmittel fuer Strassen und Wege. In: Anlehnung an DIN EN ISO 14024-Forschungsbericht 200 95 308/04; UBA-FB 000404. TEXTE 09/03; 2003

[18] Glukhovsky V. Soil Silicates. Kyiv: Gossizdat; 1959

[19] Glukhovsky V, Krivenko P, et al. Alkaline and Alkaline–Alkali-earth Hydraulic Binders and Concretes. Kyiv: Vyscha Shkola; 1979

[20] Krivenko P. Why alkaline activation–60 years of the theory and practice of alkali-activated materials. Journal of Ceramic Science and Technology. 2017;**8**(3):323-333

[21] Stanton T. Expansion of concrete through reaction between cement and aggregate. Proceedings of the American Society for Engineering Education. 1940;**66**:1781-1811

[22] Malek RIA, Roy DM. Effect of slag cements and aggregate type on alkali—Aggregate reaction and its mechanism. In: Proceedings of the 6th International Conference, Alkalies in Concrete, Research and Practice; Technical University of Denmark, Copenhagen; 22-25 June, 1983. pp. 223-230

[23] Krivenko P et al. Mechanism of preventing the alkali–aggregate reaction in alkali activated cement concretes. Cement and Concrete Composites. 2014;**45**:157-165

[24] Li Z et al. Mitigating the autogenous shrinkage of alkali-activated slag by metakaolin. Cement and Concrete Research. 2019;**122**:30-41

[25] Shi C. Alkali-aggregate reaction of alkali-slag cements. Concrete and Cement Products. 1988;**4**:14-16

[26] Nixon PJ, Sims I. RILEM Recommendations for the Prevention of Damage by Alkali-Aggregate Reactions in New Concrete Structures. RILEM State-of-the-Art Report. Dordrecht, The Netherlands: Springer; 2016

[27] Lee G, Ling TC, Wong YL, Poon CS. Effects of crushed glass cullet sizes, casting methods and pozzolanic materials on ASR of concrete blocks. Construction and Building Materials. 2011;**25**(5):2611-2618

[28] Shi C, Shi Z, Hu X, Zhao R, Chong L. A review on alkali-aggregate reactions in alkali-activated mortars/concretes made with alkali-reactive aggregates. Materials and Structures. 2015;**48**:621-628

[29] Fernandez-Jimenez A, Puertas F. The alkali–silica reaction in alkali-activated granulated slag mortars with reactive aggregate. Cement and Concrete Research. 2002;**32**:1019-1024

[30] Puertas F, Palacios M, Gil-Maroto A, Vazquez T. Alkali-aggregate behaviour of alkali-activated slag mortars: Effect of aggregate type. Cement and Concrete Composites. 2009;**31**:277-284

[31] Garcia-Lodeiro I, Palomo A, Fernandez-Jimenez A. Alkali–aggregate reaction in activated fly ash systems. Cement and Concrete Research. 2007; **37**:175-183

[32] Angulo-Ramírez DE, De Gutierrez RM, Medeiros M. Alkali-activated Portland blast furnace slag cement mortars: Performance to alkali-aggregate reaction. Construction and Building Materials. 2018;**179**:49-56

[33] Hay R, Ostertag CP. On utilization and mechanisms of waste aluminium in

mitigating alkali-silica reaction (ASR) in concrete. Journal of Cleaner Production. 2019;**212**:864-879

[34] Rashidian-Dezfouli H, Afshinnia K, Rangaraju PR. Efficiency of ground glass fiber as a cementitious material, in mitigation of alkali-silica reaction of glass aggregates in mortars and concrete. Journal of Building Engineering. 2018;**15**:171-180

[35] Shi Z, Shi C, Zhang J, Wan S, Zhang Z, Ou Z. Alkali-silica reaction in waterglass-activated slag mortars incorporating fly ash and metakaolin. Cement and Concrete Research. 2018; **108**:10-19

[36] Shi Z, Shi C, Wan S, Ou Z. Effect of alkali dosage on alkali-silica reaction in sodium hydroxide activated slag mortars. Construction and Building Materials. 2017;**143**:16-23

[37] Saha AK, Sarker PK. Mitigation of the potential alkali–silica reaction of FNS using ground FNS as a supplementary binder. Advances in Cement Research. 2019. Ahead of Print

[38] Saha AK, Sarker PK. Potential alkali silica reaction expansion mitigation of ferronickel slag aggregate by fly ash. Structural Concrete. 2018;**19**:1376-1386

[39] Saha AK, Khan MNN, Sarker PK, Shaikh FA, Pramanik A. The ASR mechanism of reactive aggregates in concrete and its mitigation by fly ash: A critical review. Construction and Building Materials. 2018;**171**:743-758

[40] Leemann A, Le Saout G, Winnefeld F, Rentsch D, Lothenbach B. Alkali–silica reaction: The influence of calcium on silica dissolution and the formation of reaction products. Journal of the American Ceramic Society. 2011; **94**:1243-1249

[41] Rumynina G, Stenchenko S. O geotermalnom sinteze shhelochnykh, shhelochezemelnykh i shhelochno-shhelochnozemelnykh alyumosilikatov v kontaktnikh zonakh shlakoshhelochnogo betona. In: Proceedings of the Poverkhnostnye Yavleniya v Disperstnykh Sistemakh. Naukova Dumka: Kiev; 1974

[42] Petrenko I, Rumynina G. Korrelyaczionnyj analiz pri issledovanii kontaktnykh zon v shlakoshhelochny'kh betonakh. In: Proceedings of the Primenenie Matematicheskogo Modelirovaniya Dlya Optimizaczii Tekhnologicheskikh i Konstruktivnykh Reshenij v Stroitel'stve; Odessa; 1975